JOURNAL OF CATALYSIS **179,** 90–99 (1998)
ARTICLE NO. CA982195

Structural and Catalytic Properties of Zeolite EMT Containing NiMo Sulfide

T. Becue,* J. Leglise,† J. M. Manoli,* C. Potvin,* and D. Cornet†,[1]

*Laboratoire de Réactivité de Surface, UMR CNRS 7609, Université P. & M. Curie, Casier 178, 4 Place Jussieu, 75252 Paris Cedex, France; †Laboratoire Catalyse et Spectrochimie, UMR CNRS 6506, ISMRA-Université de Caen, 6 Boulevard du Maréchal Juin, 14050 Caen Cedex, France

Received November 10, 1997; revised February 26, 1998; accepted May 15, 1998

This work examines bifunctional catalysts made of an acidic EMT zeolite into which Ni and Mo ions were introduced, and then sulfided. Their structure and catalytic properties were compared to those of analogous NiMo/HY. Ni and Mo were loaded onto the HEMT by wet treatment, and the solids were characterized in the calcined and sulfided state by means of XRD, porosimetry, and TEM coupled with EDX analysis. When the oxidic NiMo/EMT was sulfided, the zeolite crystals fractured in a few planar directions, and the fissures appeared to be filled with MoS_2 particles promoted with Ni. This is very different to the HY zeolite in which the sulfide slabs were scattered into the mesopores. With both supports, however, about half of the NiMo is present outside the zeolite as incompletely sulfided particles. The catalytic properties of the sulfided NiMo/EMT were examined by measuring the conversion of an *n*-heptane and benzene mixture in a flow reactor under 8 MPa hydrogen pressure. With the EMT as well as with the HY support, the rate of benzene hydrogenation varied in accordance with the amount of internal Mo. The intrinsic activity of the internal Mo matched that of a commercial $NiMo/Al_2O_3$. The NiMo/zeolites exhibited high activity for the conversion of heptane, but the cracked products exceeded by far the heptane isomers. Differences in selectivity between EMT and HY catalysts are interpreted on the basis of the balance between acidic and hydrogenation functions. © 1998 Academic Press

INTRODUCTION

Zeolite EMT is a hexagonal polytype of the cubic Y faujasite (1). The EMT structure is slightly more open than that of faujasite (2) owing to its two sets of internal cavities, connected by large apertures. Furthermore, protonic sites are easily created in zeolite EMT, and they are readily accessible to reactant molecules. Thus, EMT seems to be a good material for catalysis. Protonated EMT and Y zeolites, having a similar Al content, differ somewhat in acidity (3), because the number and strength of the sites are higher for HEMT. Both types of zeolites were tested as catalysts for the cracking of light alkanes. HEMT was more efficient than HY (4), as were the dealuminated forms (5, 6).

On the other hand, when such acidic zeolites are combined with a hydrogenation component they give rise to bifunctional catalysts which may be used in *n*-alkane hydroconversion (7–10). A Pt-loaded NaEMT catalyst performed hydrocracking of long-chain alkanes at nearly the same rate as the Pt/USY catalyst, and displayed superior branching capacity (11). EMT catalysts loaded with molybdenum oxynitride as the hydrogenating component have also been tested for the hydroconversion of heptane (12).

The present work deals with HEMT zeolites loaded with Ni and Mo, and then sulfided. Their properties as hydrocracking catalysts will be compared with those of NiMo/HY reported earlier (13) to assess the influence of the acidity and porosity of the supports. In one catalyst, phosphorus was incorporated to improve the hydrogenation function of the metal sulfide (14). All catalysts were tested for the simultaneous conversions of *n*-heptane and benzene performed under high hydrogen pressure. The location and dispersion of the phases containing Ni, Mo, and sulfur was examined by means of TEM and EDX analysis.

EXPERIMENTAL

1. Catalysts

1.1. *Zeolite EMT.* Zeolite EMT was synthesized in the sodium form using 18-crown-6 ether as template material (1), and then calcined at 673 K. The proportion of cubic domains, determined according to the criterion of Vaughan *et al.* (15), was less than 5%. This material was ion-exchanged with ammonium acetate solutions; exchange was limited to 75% of the initial Na. The ^{27}Al MAS-NMR spectra showed that all Al ions were incorporated into the zeolite lattice.

1.2. *NiMo catalysts.* Ni and Mo ions were introduced successively into the EMT support (16). Two Ni-containing precursors were obtained when the NH_4EMT

[1] To whom correspondence should be addressed. E-mail: Leglise@ismra.fr.

0021-9517/98 $25.00

TABLE 1

Chemical Composition of NiMo Catalysts

Catalyst	Zeolite structure	Si/Al (at/at) Overall[a]	Si/Al (at/at) Lattice[b]	Composition (wt%)[c] Ni	Mo	S	S/(Ni + Mo) (at/at)
E1	EMT						
Oxidic		3.7	3.9	1.7	5.4		
Sulfided		3.7	4.4	1.7	5.3	2.9	1.08
EP[d]	EMT						
Oxidic		3.8	4.2	1.8	5.4		
Sulfided		3.8	4.4	1.7	5.3	2.5	0.93
E2	EMT						
Oxidic		3.7	4.0	5.8	7.9		
Sulfided		3.7	4.4	5.6	7.7	4.8	0.85
Y1	Y						
Oxidic		3.0	4.5	2.6	8.7		
Sulfided		3.0	5.6	2.6	8.7	3.1	0.73
A1	Al_2O_3						
Oxidic				2.8	9.3		
Sulfided				2.7	9.1	4.2	0.93

[a] From chemical analysis.
[b] From NMR.
[c] Uncertainty in figures is ±0.25%.
[d] Contains 0.2% phosphorus.

was exchanged for with a nickel acetate solution (0.01 *M* for catalysts E1 and EP, 0.4 *M* for catalyst E2). The solids were dried at 353 K, then impregnated with an Mo solution by the incipient wetness technique. Catalysts E1 and E2 were treated with a solution of ammonium heptamolybdate at pH = 5.3. Catalyst EP was impregnated with a solution of $(NH_4)_6P_2Mo_{18}O_{62}$ at pH = 3.7: NMR of ^{31}P showed that 89% of the Dawson units did not change in this solution. The NiMo/HY (Y1) and NiMo/Al_2O_3 catalysts (Procatalyse HR 346, A1) were already described (16).

All NiMo catalysts were calcined in a flowing air at 773 K for 8 h. The temperature was raised slowly (50 K h^{-1}) to limit the damage to the zeolite structure. The overall compositions given in Table 1 were measured at the CNRS Analytical Division, Vernaison, France. The Ni and Mo contents in catalysts E1 and EP were lower than those in the commercial A1 catalyst. However, both these catalysts, as well as the Y1 catalyst, have the same promoter factor Ni/(Ni + Mo) as A1. Catalyst E2 had more nickel, and a slightly lower Mo content than catalyst Y1. The Na content was 1.6 wt% in the EMT catalysts, and less than 0.2% in Y1.

1.3. *Physico-chemical characterizations.* The MAS NMR spectra were recorded on a Bruker MSL 400 spectrometer. The Si/Al ratios in the lattice were deduced from the spectra of ^{29}Si. ^{27}Al spectra were used to detect nonframework aluminum. The microporous and mesoporous volumes (V_{mic} and V_{mes}) were determined from the sorption of N_2 at 77 K measured on a Micromeritics ASAP 2000 apparatus.

XRD powder patterns were recorded on a Siemens D 500 diffractometer using a Cu K_α monochromatized source. The degree of X-ray crystallinity C_e of the EMT zeolites was estimated from the intensities of all reflections in the range of 2θ between 14.5 and 23.9° (17). The C_e values for all NiMo zeolites were corrected for the absorption due to the MoO_3 phase, to assess the intrinsic crystallinity C_i of the zeolite fraction (13).

1.4. *Electron microscopy.* The catalysts were studied by means of high resolution TEM on a JEOL microscope (JEM 100 CXII) equipped with a top-entry device and operating at 100 kV. Ultramicrotome cuts (80–100 nm thick) of the samples were used. EDX analyses (STEM mode) were obtained using a LINK AN 10000 system connected to a Si-Li diode detector and a multichannel analyzer. Atomic compositions were measured on rectangular (30×40 nm^2) or circular domains (fixed STEM beam analysis, 180 or 2800 nm^2).

2. Sulfidation and Catalytic Measurements

The fixed-bed microflow reactor (16) was operated at 8 MPa hydrogen pressure; the catalyst mass was 0.17 g in all cases.

The NiMo catalysts, placed in the high-pressure reactor, were sulfided by feeding a solution containing 2 wt% of dimethyldisulfide (DMDS) dissolved in a heptane–benzene mixture (78–20). The liquid was fed at a rate of 0.14 g h^{-1} and vaporized in the hydrogen stream (0.225 mol h^{-1}). The catalyst temperature was fixed at 333 K for 18 h, and then slowly raised to 593 K. Above 450 K, the DMDS fully decomposed into H_2S and CH_4, so that sulfidation occurred at a volume ratio H_2/H_2S close to 3700. The final temperature was reached after 6 h and was kept at 593 K for one more day.

The catalytic tests were performed at 533–593 K with the same sulfur-containing feed. Reactant flow rates were 1.12×10^{-3} mol h^{-1} for heptane and 0.37×10^{-3} mol h^{-1} for benzene. The effluent gas was analyzed every 2 h with a GC equipped with a CP-SIL 19B column and a FID detector. Steady-state conditions were reached after 6 h at each temperature. No significant deactivation was found after a two week run. At the end of the run, the catalyst was cooled rapidly to room temperature. The adsorbed hydrocarbons were eliminated by further heating at 593 K (50 K h^{-1}) under an Ar flow; no elemental sulfur was evolved at this stage. After final cooling, the catalysts were withdrawn for analysis.

RESULTS AND DISCUSSION

1. Catalyst Crystallinity and Pore Volume

Upon loading Ni and Mo into NH_4EMT, the apparent crystallinty C_e was found lower than that in NaEMT, but the intrinsic C_i was higher. In parallel, a slight decrease in

TABLE 2

Structural and Textural Data of NiMo/Zeolite Catalysts

Catalyst	X-Ray crystallinity (%)		Unit-cell parameters (nm)		Internal volumes (cm^3g^{-1})[b]		
	C_e	C_i	a (±0.001)	c (±0.002)	V_{mic} (±0.005)	V_{mes} (±0.005)	V_{MO}[c]
NaEMT	100[a]	100	1.739	2.842	0.377	0.019	
E1 Oxidic	93	119	1.736	2.837	0.314	0.032	0.024
Sulfided	57	73	1.735	2.834	0.237	0.067	
EP Oxidic	92	114	1.737	2.838	0.290	0.025	0.024
Sulfided	67	83	1.735	2.834	0.270	0.041	
E2 Oxidic	88	119	1.739	2.840	0.346	0.035	0.046
Sulfided	60	82	1.738	2.839	—	—	
HY	81[a]	81	2.451		0.260	0.110	
Y1 Oxidic	60	79	2.455		0.234	0.086	0.043
Sulfided	54	72	2.449		0.206	0.064	

[a] Crystallinity of NaEMT and NaY assumed to be 100%.
[b] Volumes are expressed on a silico-aluminate basis.
[c] $NiO + MoO_3$.

unit-cell parameters was noted (Table 2). This is related to some extraction of lattice aluminum (about 7%), as confirmed by the increase in the lattice Si/Al ratio (Table 1). Furthermore, a new resonance of octahedral Al appeared at $\delta = 0$–4 ppm in the NMR spectra of the calcined NiMo zeolites (not shown here). This behavior is similar to that of the oxidic NiMo/HY, where the apparent C_e was lower than that in NaY, but the intrinsic C_i of the zeolite part equaled that in HY (81%, Table 2). Therefore, the oxidic NiMo zeolites were at least as crystalline as the protonated forms.

Upon sulfiding, all NiMo zeolites suffered partial amorphization. At this stage, C_i decreased by as much as 40% in NiMo/EMT, but only 10% in NiMo/HY. Thus, the EMT catalysts appeared to be more fragile than the NiMo/HY during sulfidation, perhaps due to their residual Na. The actual crystallinity of our catalysts is probably higher than indicated by the C_i values, because the XRD intensity reflects long-range order (18). In any case, all sulfided EMT catalysts retained substantial crystallinity, ca 70–80%.

The interior spaces available in the catalysts were estimated by measuring the volumes of micropores and mesopores. The values, expressed for 1 g of silico-aluminate, are listed in Table 2. Upon loading with NiMo and calcining, the micropore volume V_{mic} decreased in all EMT and Y zeolites. The largest changes were noted for E1 (17%) and EP (23%). There, the decrease in V_{mic} exceeded the volume V_{MO} of the bulk metal oxides (third column in Table 2). As the crystallinity C_i did not decrease, Ni and Mo ions probably entered the zeolite channels. Smaller variations of V_{mic} were observed in the metal-rich E2 (8%) and Y1 (10%) catalysts, so that part of the NiMo at least is located outside the channels in these solids.

Upon sulfiding, the micropore volume of the EMT samples further decreased by 7–25%, whereas the crystallinity C_i decreased more markedly. Meanwhile, the mesopore volume increased, showing that large voids were created in the EMT structure. Hence, although the fraction of NiMo present in the micropores cannot be ascertained, the large volume of the mesopores in the EMT catalysts may accommodate some of the metal sulfides, as was observed in NiMo/HY (13).

2. *Electron Microscopy and EDX Analysis*

2.1. *Calcined solids.* A TEM image of a thin cut of oxidic E1 is shown in Fig. 1. The large zeolite grain features two sets of well resolved fringes at intervals of 1.22 nm, corresponding to the (011) planes of the EMT. No foreign species, such as Ni and Mo oxides, or any particular defects were evident in these grains. Dark particles, about 10 nm in size, appeared to accumulate outside the zeolite grains. These particles show fringes with a 0.62 nm interval, matching the distance between the (110) planes in $NiMoO_4$. Identification of crystalline $NiMoO_4$ was confirmed by means of the diffraction pattern of selected areas (SAED), and the occurrence of a broad diffraction line at $2\theta = 14.2^\circ$ in the X-ray powder spectrum.

The oxidic E2 and EP samples displayed TEM images similar to those of E1, except for the dark particles that were found amorphous in EP.

In the calcined NiMo/EMT, the atomic compositions determined by EDX varied widely from domain to domain. However, two main types could be recognized; averaged compositions recorded for the oxidic E1 are listed in Table 3. The domains of the first type contain more Si than

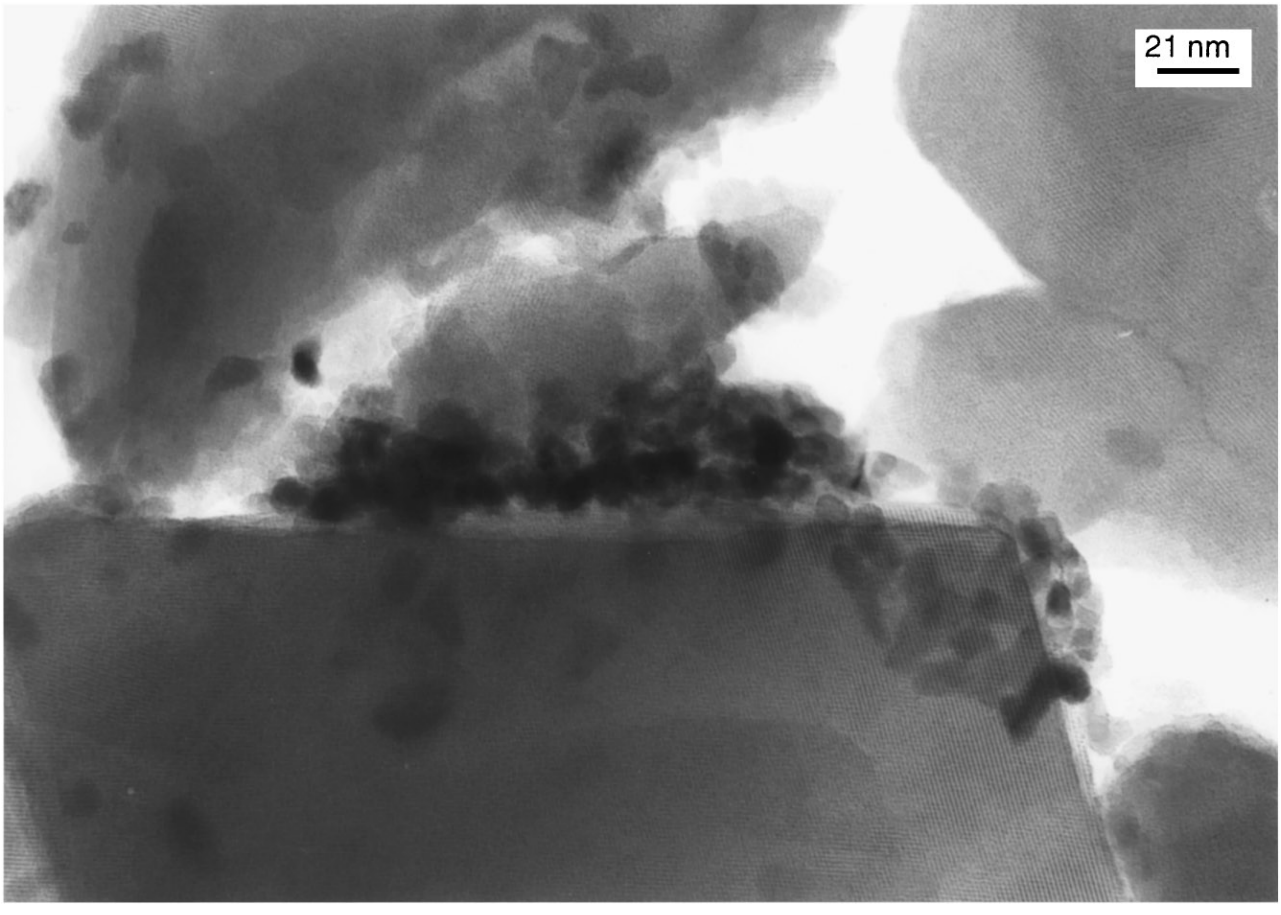

FIG. 1. TEM image of the oxidic NiMo/EMT catalyst E1 (thin cut).

the overall chemical value. They are thought to be zeolitic zones, and the Si/Al ratio higher than the overall value shows that they contain very little nonframework Al. Ni and Mo were consistently detected in such zones, with a rather uniform concentration of Ni, while that of Mo varied to a greater extent (Table 3). This proves the presence of some Ni and Mo inside the micropores or the mesopores of the zeolite.

TABLE 3

Atomic Compositions Measured by EDX on Thin Cuts of NiMo/EMT Catalyst E1

Analysis			Composition (at%)[a]				
Type	Zone	Number of analyses	Si	Al	Ni	Mo	S
			Calcined E1				
Chemical			74.4	20.0	1.9	3.6	
EDX	Zeolite	9	77.4 (1.8)	18.9 (1.9)	2.2 (0.3)	1.5 (0.6)	
	External NiMo	5	1.0 (1.0)	5.3 (3.6)	39.7 (6.5)	54.0 (4.2)	
			Sulfided E1				
Chemical			70.3	18.9	1.8	3.4	5.6
EDX	Zeolite	14	73.9 (1.2)	20.5 (0.9)	1.1 (0.3)	1.6 (0.6)	2.8 (0.9)
	External Ni	4	2.2 (2.4)	1.0 (0.6)	37.4 (0.5)	1.6 (1.1)	57.8 (1.7)
	External Mo	4	5.3 (7.9)	6.1 (3.4)	5.1 (1.6)	33.9 (2.1)	49.6 (7.6)

[a] Compositions exclude Na, C, O, and H elements. Standard deviations calculated at 95% confidence level are shown in parentheses.

The second type of domain composition was obtained when the beam focussed on dark external particles. In the calcined E1 (Table 3), such zones contained only 5% Al and virtually no Si, but appeared to be very rich in both Ni and Mo. The average Ni/Mo became established at 0.8 at/at, which was lower than expected for $NiMoO_4$. However, no external zones containing Mo without Ni could be observed, contrary to NiMo/HY, where aluminum molybdate and MoO_3 were detected outside the zeolite (13).

Similarly, the oxidic E2 sample featured two types of domains. Although this solid contained more Ni than E1, the Ni content in the zeolite zones was nearly the same as in E1. In the oxidic EP, the zeolite zones contained much less Ni than did those in E1; and the external amorphous species combined Al, Ni, and Mo with an atomic ratio Ni/Mo = 1.8.

From the atomic compositions given by EDX (c) and chemical analysis (c°), the repartition of Ni and Mo between the inside and the outside of the zeolite could be assessed (Table 4). Assuming that silicon arises exclusively in zeolite zones, the proportion P(Me) of internal metal (Ni or Mo) was calculated as

$$P(\mathrm{Me}) = \frac{c(\mathrm{Me})}{c^\circ(\mathrm{Me})}\,\frac{c^\circ(\mathrm{Si})}{c(\mathrm{Si})}.$$

In sample E1, the proportion P(Ni) is close to unity, since the 2.2 at% Ni detected inside the zeolite domains account for essentially all of the Ni introduced (Table 3). In this respect, E1 behaved like Y1. However, sample EP, which was obtained from the same precursor as E1, had P(Ni) as low as 0.32. Thus, when the Ni/EMT precursor was impregnated with the phosphomolybdate solution (instead of molybdate for E1), a large amount of Ni ions were probably back-exchanged due to the lower pH. They redeposited outside the zeolite grains as proven by the Ni/Mo ratio in the external zones of EP (1.8 instead of 0.8 for E1). Again, a low proportion P(Ni) was found in E2, but, owing to its higher loading (Table 1), this catalyst contained as much internal nickel as E1 (Table 4).

TABLE 4

Proportion P(Me) and Content of Internal Ni and Mo Deduced from EDX and Chemical Analyses

	Nickel		Molybdenum	
Catalyst	Inner content (wt%)	P(Ni)	Inner content (wt%)	P(Mo)
E1 Oxidic	1.7 ± 0.2	>0.95	2.1 ± 0.7	0.39
Sulfided	1.0 ± 0.3	0.59	2.4 ± 0.8	0.45
EP Oxidic	0.6 ± 0.2	0.32	1.6 ± 0.4	0.29
Sulfided	1.7 ± 0.5	>0.95	2.7 ± 0.9	0.52
E2 Oxidic	1.9 ± 0.2	0.33	1.5 ± 0.4	0.19
Sulfided	1.3 ± 0.4	0.23	2.6 ± 1.0	0.35
Y1 Oxidic	2.6 ± 0.2	>0.95	4.6 ± 0.5	0.53
Sulfided	1.1 ± 0.3	0.43	4.0 ± 0.9	0.46

The proportion of internal Mo was rather low in all EMT samples, ranging from 0.39 in E1 to as low as 0.19 in E2 versus 0.53 in Y1.

In summary, the internal Ni is limited to about 2 wt% in the oxidic NiMo/EMT, which is well below the exchange capacity of the NH_4 zeolite. The lower loading achieved on EP (0.6 wt%) results from the preparative procedure. Introduction of Mo appears more difficult in the EMT than in the HY zeolite, despite the larger micropore volume. The penetration of Mo ions into the EMT cavities may be restricted (19), but the near absence of mesopores in EMT is certainly another important factor.

2.2. *Sulfided catalysts.* The TEM images revealed that the NiMo/EMT catalysts were modified considerably as a result of sulfiding. The zeolite grains appeared less uniform in shape and showed two types of defects: rather small cracks and extended fissures. The irregular cracks indicated local collapse at the surface of the zeolite grain. Curled dark particles (Fig. 2) featuring the characteristic MoS_2 fringes (20–22) were associated with some of the cracks. The fissures that were found throughout the zeolite crystals were characterized by black linear streaks, identified as layers of MoS_2 slabs. Such long fissures are shown in Fig. 3 for catalyst EP; they were also evident in E1 and E2. The black streaks, about 2-nm thick, revealed that the fissures are planar defects parallel to the electron beam and oriented along the (002) planes of the zeolite. This orientation is not unique, however, since the large dark strip, 36-nm wide, seen in Fig. 3 could be associated with a defect parallel to (012) crystal planes. The MoS_2 slabs, 20–50-nm long, do not fill all the void space of the defects, in agreement with the volume of the mesopores measured in the sulfided catalysts.

In all sulfided catalysts, dark particles were found on the outer surface of the zeolite grains. They consist of MoS_2 and NiS as shown by SAED. Thus, upon sulfiding, the metal ions moved and coalesced into sulfide entities, both internal and external. During the process, the zeolite was fractured, and a limited lattice dealumination occurred (Table 1).

EDX analysis again revealed zeolitic and external zones in all sulfided NiMo/EMT. In any of the zeolitic zones, Ni and Mo were detected together (Table 4). Although no combined Ni-Mo-S or Ni sulfide phases were detected by TEM, the MoS_2 slabs, filling the defects of zeolite EMT, are probably promoted by Ni as was the case in Y1 (13).

In the external zones, EDX performed on sufficiently small domains detected either Ni sulfide or Mo sulfide in E1 and E2 (Table 3). Thus, the external $NiMoO_4$ present in these calcined solids was not apparently transformed to a mixed NiMo sulfide. In sulfided EP, phosphorus was detected, together with Al, Mo, and S, outside the zeolite.

The proportions of internal Ni and Mo were determined in the sulfided catalysts (Table 4). A comparison with the calcined solids reveals that large amounts of Ni and Mo had migrated between the interior and the exterior of the zeolite

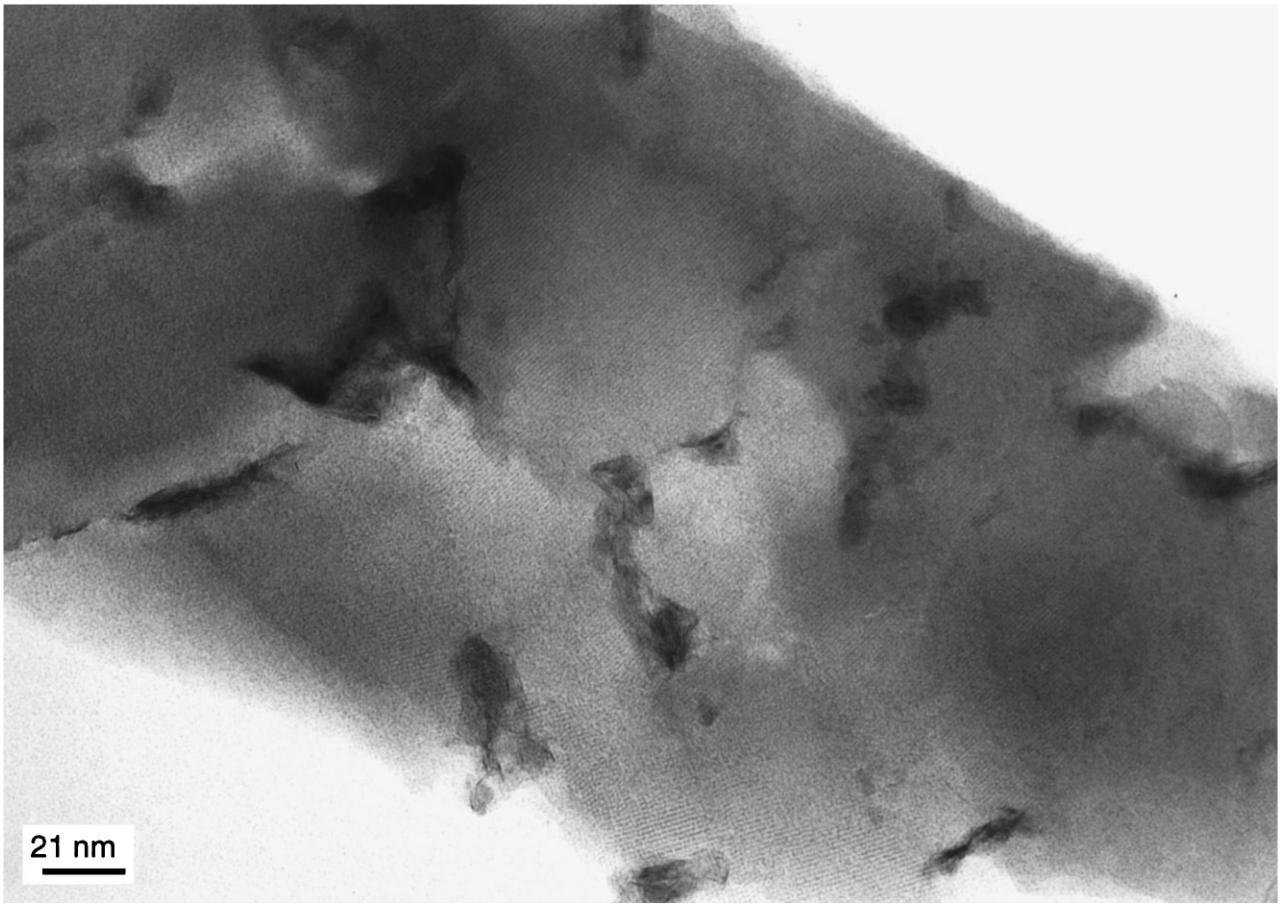

FIG. 2. TEM image of NiMo/EMT catalyst E1 sulfided at 593 K (thin cut).

upon sulfiding. Much of the internal Ni was evicted from catalysts E1 and E2, while some of the Mo moved to the interior; but the extent of migration depends on the catalyst, so that the sulfided E2 contained slightly more internal Ni and Mo than E1.

Catalyst EP behaved differently. In the oxidic form, most of the Ni and Mo was found confined to the periphery of the zeolite grains as the phosphomolybdate species generally did not decompose. These species were destroyed upon sulfiding, and, as a result, more Ni and Mo could penetrate the zeolite.

From the overall sulfur contents (Table 1), the average degree of sulfidation S/(Ni + Mo) was deduced. These values ranged between 0.73 for catalyst Y1 and 1.08 for catalyst E1, showing that, at such a high H_2/DMDS ratio (3700), sulfidation of Ni and Mo was far from being complete.

The sulfur contents in the NiMo/EMT zeolites could not be measured accurately by EDX due to overlap of the S_K and Mo_L lines. Despite this, the values reported in Table 3 for catalyst E1 suggest that the extent of NiMo sulfidation is lower in the interior than in the exterior zones. Yet in the TEM pictures, the internal MoS_2 slabs that developed at zeolite defects appeared to be well sulfided. Consequently, some of the inner metal ions, mostly Ni, remained unsulfided (13, 16). Outside the EMT, the EDX measurements were more precise due to the higher concentrations. The atomic ratios S/Ni or S/Mo varied from zone to zone, which showed that the large external particles containing Ni or Mo were not homogeneously sulfided (13).

3. *Catalytic Results*

The catalysts were evaluated by measuring the conversion of benzene at the same time as heptane. Conversion levels and product distributions were found to be stable after 12 h. The carbon contents measured after 6 days on stream were similar (about 2 wt%) for all catalysts, regardless of the zeolite or alumina support. Such low carbon levels indicate that coke has reached steady state.

3.1. *Hydrogenation of benzene.* When measuring the rate of hydrogenation of benzene, the conversion was kept very low, since the primary products, cyclohexane and methylcyclopentane, were rapidly cracked (23). At 513–533 K, cycloalkane cracking is minimal on our catalysts (24), and conversions measured in this range are thought to be representative. Apparent activation energies were identical

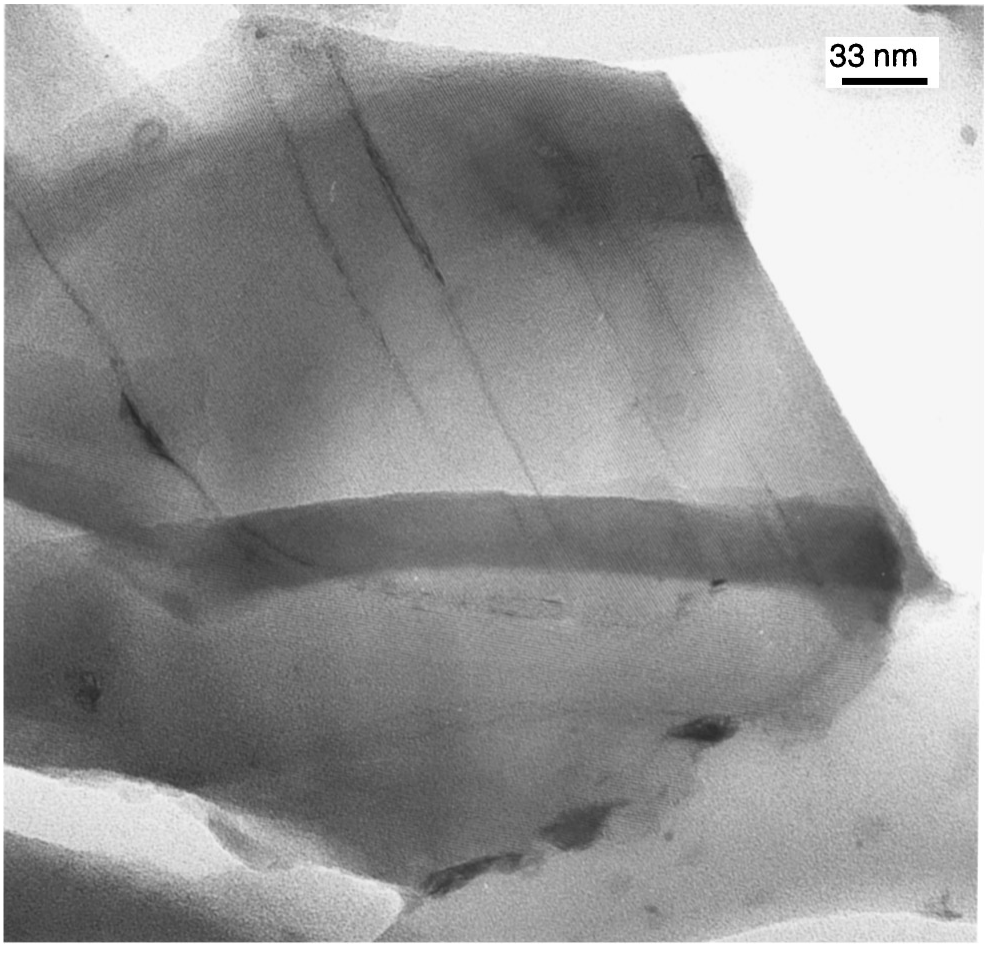

FIG. 3. TEM image of NiMo/EMT catalyst EP sulfided at 593 K (thin cut).

on the four zeolites, $E = 108 \pm 8$ kJ mol^{-1} as opposed to 76 kJ mol^{-1} for A1. The rates of hydrogenation r_A, interpolated to 553 K (Table 5) varied in the order:

$$E1 < EP < E2 < Y1 < A1.$$

The rate of hydrogenation should mainly depend on the amount of accessible Mo sites if it is assumed that sufficient Ni is present everywhere to act as a promoter. In fact, the observed rates r_A were not directly related to the overall Mo content because the NiMo/Al_2O_3, which barely contains more Mo than catalysts E2 and Y1, was clearly more active. Moreover, the internal MoS_2 particles were thin enough to ensure a much better dispersion of the metal sites than in the large external particles. Assuming the latter to be little active, the rate of hydrogenation should vary as the concentration of internal Mo (Table 3). Figure 4 shows that the rates r_A for the NiMo zeolites are nearly proportional to the amount of internal Mo. Moreover, the NiMo/Al_2O_3 fits on the line when its Mo content is restricted to the fraction that could be extracted by acid (25).

TABLE 5

Rates of Reaction (mol h^{-1} g^{-1}) Measured at 553 K for the Simultaneous Conversion of Benzene (r_A) and Heptane (r_{HC})

Catalyst	E1	EP	E2	Y1	A1
r_A (benzene)	17	27	32	48	76
10^{-3} r_{HC} (heptane)	1.7	2.0	2.8	2.7	<0.01

In conclusion, although the inner metal sulfides may differ in composition and texture depending on the EMT or HY support, the NiMo zeolites possess intrinsic activities close to that of the alumina catalyst. The higher activity of Y1 compared with EMT merely results from an easier incorporation of Mo sulfide into the faujasite structure.

3.2. *Hydrocracking of heptane: Comparison of activity.* Heptane did not react over catalyst A1, but all zeolite catalysts converted heptane much faster than benzene. Products were light alkanes, mainly propane and isobutane, and heptane isomers. Conversions of heptane measured at constant flow rates are plotted in Fig. 5A for different temperatures. Catalysts Y1 and E2 were clearly more efficient than E1 and EP, and again catalyst EP

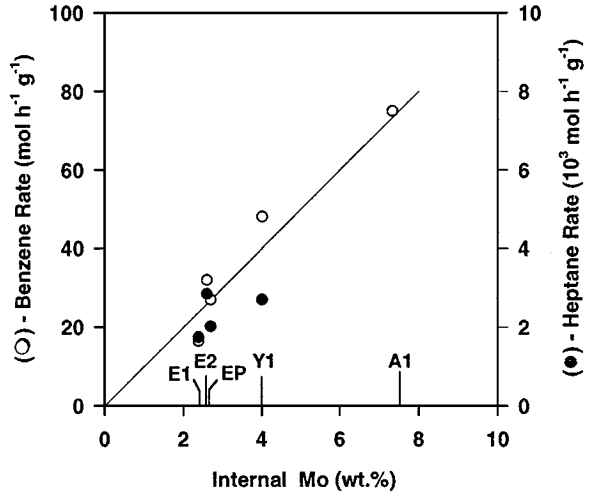

FIG. 4. Relationship between rates of reaction at 553 K and amount of internal Mo: r_A; hydrogenation of benzene (○; left scale); r_{HC}; hydroconversion of heptane (●; right scale).

(ex-phosphomolybdate) was more active than E1. Apparent activation energies deduced from these curves are close to $E = 140 \pm 8$ kJ mol^{-1}. The rates of heptane hydroconversion r_{HC}, measured at 553 K, are listed in Table 5. The trend in heptane conversion,

$$E1 < EP < Y1 < E2,$$

is the same as in the hydrogenation of benzene, at least within the EMT series. Such a parallel is to be expected when the hydrogenation capacity is a limiting factor of hydrocracking activity. However, the relationship between r_{HC} and internal Mo is not as general as for the rate of hydrogenation (Fig. 4). Catalyst Y1 is different from the NiMo/EMT, featuring a lower r_{HC}/r_A ratio. Therefore, the rate r_{HC} depends to some extent on the zeolite structure, which determines both the acidity and the rate of transport within the channels.

3.3. *Selectivity in heptane hydroconversion.* Over all NiMo zeolites, the conversion of heptane was strongly oriented toward cracking, and cracked products appeared already at very small conversion. This is shown in Fig. 5B, where the conversion to heptane isomers is plotted against the yield of cracked products. A maximum of 13% isomers was found on catalyst Y1, but only 9% on E2, and even less on E1 and EP.

The distribution of heptane isomers was nearly constant at all conversions from 5% to 90%. On any of the three NiMo/EMT, the isomers were 75% monobranched (MB) and 25% dibranched (DB). The NiMo/HY catalyst gave nearly the same distribution, with 74% MB and 26% DB. However, the nature of the MB isomers was slightly different, as the ratio 2-methyl/3-methylhexane was 0.85 for the NiMo/EMT catalysts, and only 0.75 for Y1.

The distributions of cracked products were quite similar on all NiMo/zeolites. For 100 moles C_7 cracked, 90 moles C_3; 96 C_4; 4 C_5; and 2 C_6 were obtained, i.e. a total of 192 moles. Thus, aside from a simple splitting, $C_7 \rightarrow C_3 + C_4$, some bimolecular cracking (26) occurred. Indeed, the cracked C_4-C_5-C_6 had predominantly branched structures. This tendency was higher on the EMT catalysts. For instance, the ratio i-C_4/n-C_4 was found equal to 17 for NiMo/EMT, compared to 12.5 for NiMo/HY.

4. *Discussion*

The Ni and Mo ions, inserted into the acidic zeolites EMT, and then sulfided, led to a stable activity in hydrocarbon conversion, since coke formation was limited. The isomerized and cracked products are similar to those found with

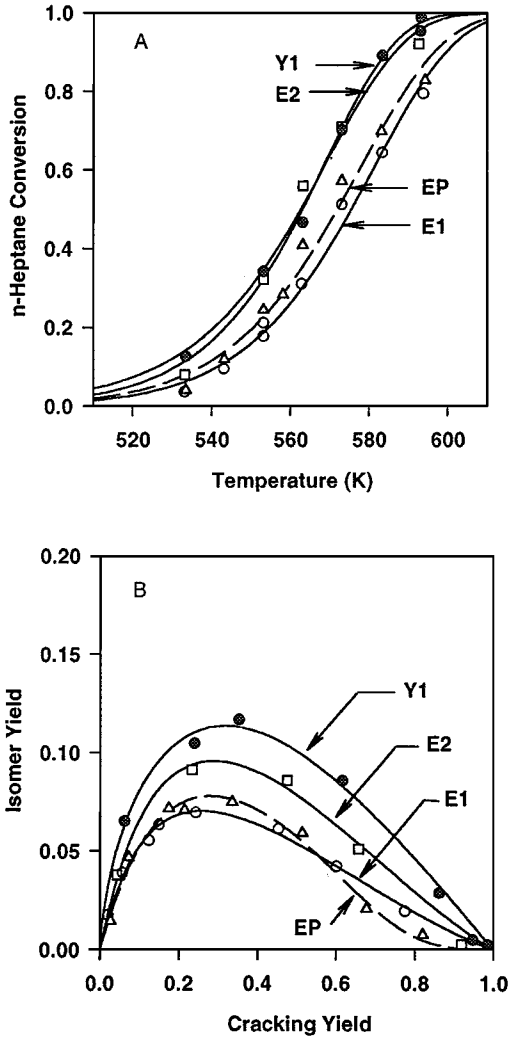

FIG. 5. Hydroconversion of n-heptane over the NiMo/zeolite catalysts at constant feed rate (0.76 g g_{cat}^{-1} h^{-1}) – $P_{Hp} = 36$ kPa, $P_{H2} = 8$ MPa: (A) conversion as a function of reaction temperature; (B) selectivity diagram; yield of isomers versus yield of cracked products.

a cracking catalyst (27). The metallic function in the NiMo zeolites is unable to balance the strong acidic function, so that the rate of hydrocracking r_{HC} hardly depends on the type of zeolite, EMT or Y.

The bifunctional character of the NiMo/HY catalysts has, however, been established (24). The promoted Mo sulfide provides the sites necessary for the dehydrogenation of heptane into *n*-heptene, but this alkene has to migrate to an internal acidic site to adsorb as a carbenium ion $n\text{-}C_7H_{15}^+$:

$$n\text{-}C_7H_{14} + H^+ \rightleftarrows n\text{-}C_7H_{15}^+ \qquad \text{(step p)}$$

or

$$n\text{-}C_7H_{14} + C_xH_{2x+1}^+ \rightleftarrows n\text{-}C_7H_{15}^+ + C_xH_{2x}. \qquad \text{(step d)}$$

The classical sequence (27–29) states that the linear C_7^+ is rapidly isomerized:

$$n\text{-}C_7H_{15}^+ \rightleftarrows iso\text{-}C_7H_{15}^+; \qquad \text{(step i)}$$

then the branched carbenium ion is either split to light products, e.g.,

$$iso\text{-}C_7H_{15}^+ \rightarrow C_3H_6 + iso\text{-}C_4H_9^+ \qquad \text{(step c)}$$

or desorbed as isomerized alkene through step d.

The formation of heptane isomers depends on step d; thus, the selectivity isomerization-to-cracking relies on the relative rates of steps c and d. Experiments with mechanical mixtures of $NiMo/Al_2O_3$ and zeolite HY showed that alkene migration from the outside to the inside of the zeolite was slow. In the NiMo zeolites, the alkene involved in step d is mainly produced on the internal metallic sites, and its concentration is not high enough to cause desorption to occur at a faster rate than cracking, particularly for the dibranched carbenium ions. Furthermore, some of the isoheptenes produced may be readsorbed and cracked before they can reach the metallic sites. Cracking is thus strongly favored over isomerization for the EMT catalysts, as well as for the Y, and the cracked products are highly branched.

However, the selectivity of the NiMo/EMT catalysts differed slightly from that of the NiMo/HY, notably by a lower yield of isomers. The TEM images showed that the metal sulfide was concentrated in a few places (fissures) inside EMT, but was better spread in the mesopores in HY. The average distance between hydrogenating and acidic sites is likely to be longer in the NiMo/EMT than in the NiMo/HY. This tends to reduce the concentration of alkene at the acidic sites, making the selectivity of the NiMo/EMT closer to that of a cracking catalyst. The same factor is expected to reduce the hydrocracking activity, but its influence may be compensated for by the stronger acidity of the EMT.

CONCLUSION

Similarities and differences between the NiMo catalysts based on EMT and HY zeolites are summarized as follows:

The NiMo zeolites treated under typical industrial conditions (HC/H_2S ratio) were incompletely sulfided, but the extent of sulfidation was similar to that of $NiMo/Al_2O_3$. In all sulfided zeolites, Ni and Mo were shared between the interior and exterior of the zeolite. The proportion of internal Mo in EMT was lower than in HY. The Mo sulfide formed at structural defects inside the zeolite and was probably promoted by Ni. In zeolite EMT, small MoS_2 particles concentrated in the extended fissures created by the sulfidation, whereas they were dispersed in the mesopores of the stabilized HY.

All catalysts were characterized by a stable activity in hydrocarbon conversion under high hydrogen pressure. The capacity for benzene hydrogenation correlated well with the amount of internal Mo, although the morphology of the sulfide differed on both supports. For the hydroconversion of heptane, however, the hydrogenation function is insufficient to balance the strong acidity of the supports. Thus, cracking was favored at the expense of isomerization, and the tendency was more pronounced with the EMT than with the HY.

ACKNOWLEDGMENTS

The help of Mrs. P. Beaunier and Mr. M. Lavergne with the TEM and STEM-EDX measurements is greatly appreciated.

REFERENCES

1. Delprato, F., Delmotte, L., Guth, J. L., and Huve, L., *Zeolites* **10**, 546 (1990).
2. Baerlocher, C., McCusker, L. B., and Chiapetta, R., *Micropor. Mat.* **2**, 269 (1994).
3. Su, B. L., Manoli, J. M., Potvin, C., and Barthomeuf, D., *J. Chem. Soc. Faraday Trans.* **89**, 857 (1993).
4. Douguier, F., Patarin, J., Guth, J. L., and Anglerot, D., *Zeolites* **12**, 160 (1992).
5. Zholobenko, V., Garforth, A., Marakova, M., Zhao, J., and Dwyer, J., *in* "Catalysis by Microporous Materials" (H. K. Beyer, H. G. Karge, I. Kiricsi, and J. B. Nagy, Eds.), Stud. Surf. Sci. Catal., Vol. 94, p. 560. Elsevier, Amsterdam, 1995.
6. Lischke, G., Schreier, E., Parlitz, B., Pitsch, I., Lhose, U., and Woettke, M., *Appl. Catal. A* **129**, 57 (1995).
7. Schulz, H. F., and Weitkamp, J., *Ind. Eng. Chem. Prod. Res. Dev.* **11**, 46 (1972).
8. Maxwell, I. E., *Catal. Today* **1**, 385 (1987).
9. Thomazeau, C., Canaff, C., Lemberton, J. L., Guisnet, M., and Mignard, S., *Appl. Catal. A* **103**, 161 (1993).
10. Welters, W. J. J., van der Waerden, O. H., de Beer, V. H. J., and van Santen, R. A., *Ind. Eng. Chem.* **34**, 1166 (1995).
11. Martens, J. A., Tielen, M., and Jacobs, P. A., *in* "Zeolites as Catalysts, Sorbents and Detergent Builders" (H. C. Karge and J. Weitkamp, Eds.), Stud. Surf. Sci. Catal., Vol. 46, p. 49. Elsevier, Amsterdam, 1989.
12. Becue, T., Manoli, J. M., Potvin, C., and Djega-Mariadassou, G., *J. Catal.* **170**, 123 (1997).
13. Leglise, J., Manoli, J. M., Potvin, C., Djega-Mariadassou, G., and Cornet, D., *J. Catal.* **152**, 275 (1995).

14. Topsøe, H., Clausen, B. S., and Massoth, F. E., *in* "Hydrotreating catalysis, Science and Technology," Springer-Verlag, Berlin, 1996.
15. Vaughan, D. E. W., Treacy, M. M. J., Newsam, J. M., Strohmaier, K. G., and Mortier, W. J., *in* "Zeolite Synthesis" (M. L. Occelli and H. E. Robson, Eds.), A.C.S. Symp. Ser., Vol. 398, p. 544. Am. Chem. Soc., Washington, DC, 1989.
16. Leglise, J., Janin, A., Lavalley, J. C., and Cornet, D., *J. Catal.* **114**, 388 (1988).
17. Chatelain, T., Patarin, J., Soulard, M., Guth, J. L., and Schultz, P., *Zeolites* **15**, 90 (1995).
18. Mauge, F., Courcelle, J. C., Engelhard, P., Gallezot, P., Grosmangin, J., Primet, M., and Trusson, B., *in* "Zeolites Synthesis, Structure, Technology & Application" (B. Drzaj, S. Hocevar, and S. Pejovnick, Eds.), Stud. Surf. Sci. Catal., Vol. 24, p. 285. Elsevier, Amsterdam, 1985.
19. Welters, W. J. J., Vorbek, G., Zandbergen, H. H., van de Ven, L. M. J., van Oers, E. M., de Haan, J. W., de Beer, V. H. J., and van Santen, R. A., *J. Catal.* **161**, 819 (1996).
20. Delannay, F., *Appl. Catal.* **16**, 135 (1985).
21. Pratt, K. C., Sanders, J. V., and Christov, V., *J. Catal.* **124**, 416 (1990).
22. Chianelli, R. R., Ruppert, A. F., Yacamán, M. J., and Vázquez-Zavala, A., *Catal. Today* **23**, 269 (1995).
23. Chen, J. K., Martin, A. M., Kim, Y. G., and John, V. T., *Ind. Eng. Chem. Res.* **27**, 401 (1988).
24. Cornet, D., El Qotbi, M., and Leglise, J., *in* "Proceedings 1st Int. Symp./6th Eur. Workshop on Hydrotreatment and Hydrocracking of Oil Fractions, Oostende, 1997" (G. F. Froment, B. Delmon, and P. Grange, Eds.), Stud. Surf. Sci. Catal., Vol. 106, p. 147. Elsevier, Amsterdam, 1997.
25. Bachelier, J., Tilliette, M. J., Duchet, J. C., and Cornet, D., *J. Catal.* **87**, 292 (1984).
26. Leglise, J., El Qotbi, M., and Cornet, D., *Collec. Czech. Chem. Commun.* **57**, 882 (1992).
27. Giannetto, G., Perot, G., and Guisnet, M., *Ind. Eng. Chem. Prod. Res. Dev.* **25**, 481 (1986).
28. Weitkamp, J., and Ernst, S., *in* "Guidelines for Mastering the Properties of Molecular Sieves" (D. Barthomeuf, E. G. Derouane, and W. Hölderich, Eds.), Nato ASI Ser. B: Physics, Vol. 221, p. 343. Plenum, New York, 1990.
29. Martens, J. A., Jacobs, P. A., and Weitkamp, J., *Appl. Catal.* **20**, 239 (1986).